

According to our estimates $c/\Gamma \sim 0.03$ cm, in which case (10) is easily satisfied for most laser beams, and (5) is valid.

The second point that I wish to make concerns beam degradation. The production of effective photons according to (1) is an irreversible process—they do not return to the original beam frequency after passing through the focal spot. The effect of (1) is to increase the entropy of the beam. Not only does the frequency distribution broaden, but the beam collimation is also destroyed; therefore, the beam very quickly dissipates and is lost.⁷ One expects that the time scale for this process is inversely proportional to the product $I\Gamma$, since the reaction rate is directly proportional to the product of density and cross section. For high-intensity lasers, the intensity may be three to six orders of magnitude larger than gas-breakdown thresholds. Consequently, the rate of increase in entropy of the beam should be extremely rapid for high-intensity beams; the scaling law gives $\tau_{\text{eff}} \sim 10^{-2}$ ps or smaller. Because the time required to produce significant numbers of effective photons is simply related to the rate of entropy increase, one expects that any laser beam of appreciable intensity will tend to break up and lose its frequency and direction definition. This clearly does not happen. Laser beams may pass through focal spots where the intensity is very high, and yet remain essentially diffraction limited. There is very little increase in entropy

due to focusing them. Consequently, I must conclude that the randomization of the beam implied by (1) and (8) does not occur.

In conclusion, I have shown that process (1) is in conflict with two experimental results: The photon-photon cross-section (9) is clearly far too large, and laser beams do not randomize on being focused to a high intensity. Consequently process (1) cannot be accepted. The apparent success of effective-photon theory in laser-induced gas breakdown is either an empirical result with no fundamental basis, or a result for which it has a basis other than (1).

The author is grateful to A. Szoke for helpful discussions.

^(a)Work performed under the auspices of the U. S. Energy Research and Development Administration under Contract No. W-7405-Eng-48.

¹E. Panarella, *Found. Phys.* **4**, 227 (1974).

²E. Panarella, *Phys. Rev. Lett.* **33**, 950 (1974).

³E. Panarella, *Can. J. Phys.* **54**, 1815 (1976).

⁴Ref. 3, Appendix.

⁵A. A. Abrikosov, L. P. Gorkov, and I. Y. Dzyaloshinski, *Quantum Field Theoretic Methods in Statistical Physics* (Pergamon, New York, 1965).

⁶An example of this approach in electron scattering is given by E. P. Tryon, *Phys. Rev. Lett.* **32**, 1139 (1974).

⁷The beam is beginning its approach to thermal equilibrium, i.e., maximum entropy.

Spatially Resolved α Emission from Laser Fusion Targets^(a)

N. M. Ceglio and L. W. Coleman

Lawrence Livermore Laboratory, University of California, Livermore, California 94550

(Received 2 February 1977)

The α -particle emission from laser-compressed, D-T-filled microspheres has been imaged using a zone-plate-coded imaging technique. Nominal image resolution was 10 μm . Approximately 97% of the recorded α emission was found to originate within a thermonuclear burn region of diameter roughly $\frac{1}{3}$ that of the original target. The full width at half-maximum of the burn region had a diameter roughly $\frac{1}{6}$ that of the target.

The central concept in inertial-confinement fusion is the implosion of hydrogen-isotope fuel to thermonuclear burn conditions.¹ Experimental programs exist in a number of laboratories throughout the world to test the viability of using powerful laser systems to drive such implosions. Exploding pusher² target experiments involving laser implosion of D-T-filled glass microspheres have produced modest compression of the laser target,³ fusion yields in excess of 7×10^8

reactions,⁴ confirmation of the thermonuclear origin of the fusion reactions,⁵ and indirect evidence that the detected thermonuclear reaction products originate within the compressed core (as opposed to the corona) of the imploded target.⁵ There has been, however, no explicit demonstration that the thermonuclear burn occurs within the compressed target core, nor had the spatial distribution of the fusion events within the burn region been measured.

This Letter reports the first high-resolution ($\sim 10 \mu\text{m}$), direct images of the thermonuclear burn region within laser fusion targets. Specifically, the α emission from laser-compressed, D-T-filled microspheres has been imaged using a coded imaging technique, zone-plate-coded imaging (ZPCI).⁶ Nominal image resolution was $10 \mu\text{m}$. The size of the thermonuclear burn region and the spatial distribution of the α emission within the compressed target were measured. These measurements provide an explicit demonstration that the thermonuclear burn produced by laser-driven implosions does indeed occur within a compressed core of the imploded target.

α imaging experiments were conducted using the Argus laser-target irradiation facility at Lawrence Livermore Laboratory. This laser system produces a dual-beam, multiterawatt pulse of $1.064\text{-}\mu\text{m}$ radiation. Typical pulse duration is 25–60 psec (full width at half-maximum) with 50–80 J per beam. The laser output is focused onto a target using a pair of $f/1$ aspheric lenses. The standard target used in these experiments was a glass microsphere (typical o.d. of 80–100 μm with submicron wall) filled with an equimolar D-T gas mixture.⁷

High-resolution imaging of the α emission from laser-imploded targets was accomplished using a coded imaging technique, ZPCI.^{8,9} The viability of ZPCI for high-resolution microscopy of x-ray and charged-particle emissions from sources of limited extent (source area \ll zone-plate area) has been recently demonstrated.^{10,11} Extensive discussion of the theoretical and experimental details of ZPCI are provided elsewhere.^{10–14} A brief summary follows.

ZPCI is a two-step imaging technique. In the first step the radiation source to be imaged casts a shadowgraph (coded image) through a Fresnel-zone plate (coded aperture) onto an appropriate detector. Image reconstruction (second step: shadowgraph decoding) is achieved via procedures similar to those used in holography. An appropriate photographic transparency is produced from the original shadowgraph; the shadowgraph transparency is then illuminated with a coherent light source. The Fresnel diffraction pattern of the transmitted light produces (downstream of the transparency) a reconstruction of the original source distribution—inverted and magnified.

Use of a coded imaging technique is appropriate for low-intensity source distributions because it allows for high-resolution imaging while main-

taining a large solid angle for radiation collection. Specifically, the resolution capability of ZPCI is limited only by the width of the narrowest zone of the coded aperture, whereas the solid angle for radiation collection varies as the coded aperture area. So then, a coded aperture of many zones with a microscopically narrow outermost zone will provide high resolution in addition to high radiation-collection efficiency.

The zone-plate camera viewed the target in a plane normal to the directions of the two-sided laser irradiation. It provided an overall image magnification factor of 5.4. The coded aperture used for α imaging was a free-standing Fresnel-zone-plate structure of 100 zones. It subtended a solid angle for radiation collection of approximately 2×10^{-2} sr. (The target-to-zone-plate distance was ~ 1 cm.) The zone-plate material was gold, $\geq 5 \mu\text{m}$ thick. The width of the narrowest zone was $5.3 \mu\text{m}$. Details of zone-plate fabrication are provided elsewhere.¹⁴

The coded α image was recorded in a $6\text{-}\mu\text{m}$ -thick cellulose nitrate film, a threshold-type ion track detector commonly used in α autoradiography.¹⁵ A $7.6\text{-}\mu\text{m}$ -thick Be foil was placed in front of and in intimate contact with the cellulose nitrate. It served to stop heavy-ion species (Si, O, C) from reaching the polymer film. A series of discrimination experiments was conducted which explicitly confirmed that the recorded coded images were produced by α particles and not other radiation species.^{16,17}

α images were recorded for a number of laser-imploded microsphere targets. Data from two representative experiments (designated *A* and *B*) are listed in Table I. Figure 1 shows the coded image recorded on shot *B*. It represents the raw data of the imaging experiment. It is a coded array of 1.3×10^6 pinholes (typically $1\text{--}2 \mu\text{m}$ diameter) through the cellulose nitrate layer. Each pinhole was produced by an α track through the $6\text{-}\mu\text{m}$ -thick polymer. The measured α track density in the coded image was found to be in excellent agreement with that expected from the α yield and the solid angle subtended by the coded aperture.

Figures 2(a) and 2(b) are two-dimensional (2D) contour maps of the reconstructed α images recorded on shots *A* and *B*, respectively. Each contour represents a focus of constant α -emission density (time-integrated intensity); the incremental change in α emission is constant between successive contours. The thermonuclear-burn-region dimensions cited in Table I are

TABLE I. Target-, laser-, and thermonuclear-burn data are presented for two representative α imaging experiments. The thermonuclear burn region had an ovoid shape. The dimensions presented are measured along the vertical and horizontal axes (respectively) of the oval. The imaging geometry was such that the vertical axis was normal to and the horizontal axis collinear with the directions of the two-sided laser irradiation of the target.

	Target diameter (μm)	Target wall (μm)	D-T fill (mg/cm^3)	Laser power (W)	Pulse width (FWHM) (psec)	Neutron yield	Burn region dimensions (μm)	Burn region (FWHM) (μm)
A	86	0.64	1.58	2.4×10^{12}	50	$(3.1 \pm 0.6) \times 10^8$	29; 26	16; 16
B	88	0.88	3.10	3.9×10^{12}	27	$(8 \pm 1) \times 10^8$	26; 22	18; 15

measured from the outermost contour in Figs. 2(a) and 2(b). The region of thermonuclear burn was found to have an ovoid shape of diameter roughly one-third that of the original target. An estimate of the α emission originating outside the contour map regions was made by counting the α -track density in the appropriate penumbra regions of the respective shadowgraphs. It was concluded that on shot A no more than 4% and on shot B no more than 10% of the total α emission could have originated outside the respective contour-map regions.

Scans of the α -emission density taken along horizontal and vertical lines through the center of each of the contour maps in Fig. 2 provided estimates of the FWHM for the spatial distribution of the α emission. The FWHM of the burn region was roughly one-sixth of the original target diameter. These measured values are listed in Table I.

The data of Table I and Fig. 2 directly demonstrate that the thermonuclear burn occurred with-

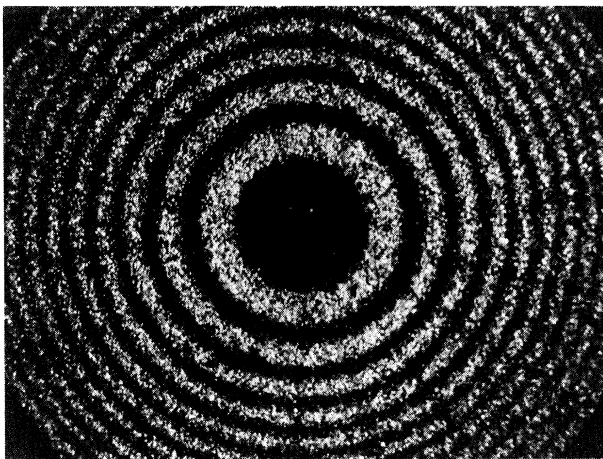


FIG. 1. Coded image of the α emission recorded on shot B. It is an array of more than one million pinholes (each produced by an α track) through the cellulose nitrate layer.

in the compressed core and not in the corona of the laser-compressed targets. The measurements imply target-volume-compression factors of order 50 and therefore mean D-T fuel densities of order $0.2 \text{ g}/\text{cm}^3$. These results agree with 2D computer-code simulations of these laser-driven implosion experiments and thus support the calculational models.¹⁸ In addition, the measured size of the compressed D-T burn region is in general agreement with α pinhole-camera data.⁸

The contour maps in Fig. 2 show the thermonuclear burn region to have an ovoid shape with the eccentricity of the oval increasing with increased

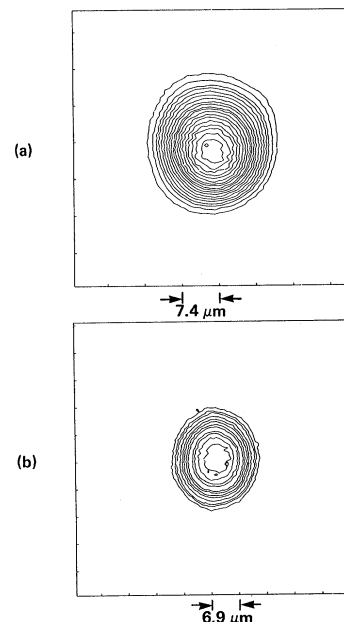


FIG. 2. Two-dimensional isoemission contour maps of the reconstructed α images recorded on shots A and B are presented in (a) and (b) respectively. The isoemission maps were obtained from microdensitometer traces of the photographically recorded, reconstructed images. The film density contours were converted to α -emission contours, taking into account film nonlinearities. The images are scaled in source dimensions.

TABLE II. Parameters and results of a crude calculation of the thermonuclear yield using α imaging results.

	Ion temperature (keV)	Ion density ($N_D = N_T$) (cm^{-3})	Reaction rate ($\text{cm}^{-3} \text{sec}^{-1}$)	Burn time (psec)	Calculated yield	Measured yield
A	5.6	5.6×10^{21}	6.3×10^{26}	36	2.6×10^8	$(3.1 \pm 0.6) \times 10^8$
B	7.0	1.7×10^{22}	1.2×10^{28}	27	2.4×10^9	$(8 \pm 1) \times 10^8$

laser power on target—a trend that is consistent with 2D computer-code analyses.¹⁸ The measured shape of the burn region is also in good agreement with time-integrated x-ray microscope images of the compressed core of the target.¹⁹

The consistency of the α -imaging results with the measured thermonuclear yield may be illustrated by a crude but reasonable calculation of the anticipated yield using the data of Table I. The thermonuclear burn region is modeled as a constant-temperature, equimolar D-T mixture compressed to the burn-region dimensions given in Table I. The effective temperature is obtained from α and neutron time-of-flight spectrometer data; ion density is assumed equal to the original fuel density multiplied by the volume compression ratio; and the burn time is taken as the ratio of burn-region diameter to mean ion sound velocity. The parameters for and results of this simple calculation for experiments A and B are represented in Table II. The calculated thermonuclear yield is in both cases within a factor of 3 of the measured values.

The size and shape of the D-T burn region of compressed, laser-driven fusion targets have been measured by the ZPCI α imaging technique and the concurrence of the results with the measured fusion yield, x-ray microscope, and α pinhole-camera data, and 2D computer-code simulations has been demonstrated. Further imaging studies are continuing in which the ZPCI technique is being used to image the suprathreshold x-ray and fast-ion emission from laser-imploded targets.

It is a pleasure to acknowledge the contributions of the following Lawrence Livermore Laboratory personnel: H. G. Ahlstrom, D. T. Attwood, M. J. Boyle, C. Dittmore, R. Griffith, W. Hermann, B. Holloway, J. Houghton, J. T. Larsen, R. A. Lerche, J. H. Nuckolls, G. Stone, E. K. Storm, G. Tirsell, and the Argus laser team.

^(a)Work performed under the auspices of the U. S. Energy Research and Development Administration under Contract No. W-7405-Eng-48.

¹J. Nuckolls, L. Wood, A. Thiessen, and G. Zimmerman, *Nature (London)* **239**, 139 (1972); K. A. Brueckner, P. M. Campbell, and R. A. Grandey, *Nucl. Fusion* **15**, 471 (1975).

²J. H. Nuckolls, in *Progress in Lasers and Laser Fusion*, edited by B. Kursunoglu (Plenum, New York, 1975), pp. 105–116.

³P. M. Campbell, G. Charatis, and G. R. Montry, *Phys. Rev. Lett.* **34**, 74 (1975).

⁴E. K. Storm, *Bull. Am. Phys. Soc.* **21**, 1173 (1976).

⁵V. W. Slivinsky, H. G. Ahlstrom, K. G. Tirsell, J. T. Larsen, S. Glaros, G. Zimmerman, and H. Shay, *Phys. Rev. Lett.* **35**, 1083 (1975).

⁶N. M. Ceglio and E. V. George, *Bull. Am. Phys. Soc.* **20**, 1350 (1975).

⁷Lawrence Livermore Laboratory, Laser Program Annual Report—1975, No. UCRL 50021-75 (unpublished), pp. 42, 75.

⁸On this same series of experiments the α emission from the glass microsphere was also imaged by an alternative technique, the pinhole camera [see V. W. Slivinsky, K. M. Brooks, H. G. Ahlstrom, E. K. Storm, H. N. Kornblum, and G. R. Leipelt, to be published].

⁹Slivinsky, Brooks, Ahlstrom, Storm, Kornblum, and Leipelt, Ref. 8.

¹⁰N. M. Ceglio, *J. Appl. Phys.* **48**, 1563 (1977).

¹¹N. M. Ceglio, D. T. Attwood, and E. V. George, *J. Appl. Phys.* **48**, 1566 (1977).

¹²L. Mertz and N. O. Young, in *Proceedings of the International Conference on Optical Instrumentation* (Chapman and Hall, London, 1961), p. 305; H. H. Barrett and F. A. Horrigan, *Appl. Opt.* **12**, 2686 (1973).

¹³H. I. Smith and N. M. Ceglio, *Bull. Am. Phys. Soc.* **21**, 1078 (1976).

¹⁴N. M. Ceglio and H. I. Smith, "Micro Fresnel Zone Plates for Coded Imaging Applications" (to be published).

¹⁵R. L. Fleischer, P. B. Price, and R. M. Walker, *Nuclear Tracks in Solids* (Univ. of California Press, Berkeley, 1975).

¹⁶The radiation discrimination achieved deserves further explanation. α particles incident on the cellulose nitrate (CN) in this experiment produced ionization tracks passing through the 6- μm layer. Subsequent etching of the CN transformed the α ionization channels into microscopic pinholes passing *all the way through*

the polymer. X rays and electrons do not produce tracks in CN. Hydrogenic ions are capable of producing only short ($< 6 \mu\text{m}$) ionization tracks in CN. Such tracks are *not* transformed into pinholes passing *all the way through* the CN layer by the etch procedures. Thus, the pinhole array recorded in the polymer detector (Fig. 1) is in fact representative of the spatial distribution of α particles incident on the CN film.

¹⁷N. M. Ceglio, "Zone Plate Coded Imaging of Alpha Particle Emission from Laser Fusion Targets" Lawrence Livermore Laboratory, Laser Program Annual

Report, 1976 (unpublished), Article I.B.3i.

¹⁸J. T. Larsen, Bull. Am. Phys. Soc. **20**, 1267 (1975).

¹⁹The FWHM dimensions of the central region of the compressed target taken from x-ray microscopic images (at $\sim 4 \text{ keV}$) of the imploded shell are ($32 \mu\text{m}$, $31 \mu\text{m}$) for shot A and ($40 \mu\text{m}$, $32 \mu\text{m}$) for shot B along the vertical and horizontal axes respectively. The agreement between the eccentricities measured from FWHM α imaging data and FWHM x-ray imaging data is within experimental uncertainty, and illustrates the similarity in shape of the two types of images

Geometric Focusing of 20-GW Proton Beams with Use of a Magnetically Insulated Diode

M. Greenspan, S. Humphries, Jr., J. Maenchen, and R. N. Sudan
Laboratory of Plasma Studies, Cornell University, Ithaca, New York 14853
 (Received 14 March 1977)

We have obtained initial geometric-focusing results using a high-current ($\geq 100 \text{ kA}$) magnetically insulated diode. At the line focus, current densities over 300 A/cm^2 have been obtained with a radial compression of about 10. Results for propagation of the intense beams are in excellent agreement with geometric single-particle predictions.

Studies of the propagation of proton beams produced by a high-power, magnetically insulated diode ($> 100 \text{ kA}$ at up to 300 kV) are described in this Letter. The diode is a major scale-up of previous work.¹ The chief developments in the present experiment were the following: (a) An order-of-magnitude increase in current output was achieved over that previously reported for magnetically insulated diodes^{1,2} while preserving the virtues of high efficiency and low electrode damage. (b) An extraction cathode of thickness larger than the skin depth for the pulsed insulating magnetic field was used so that the field was confined to the anode-cathode gap. Thus the region interior to the cylindrical cathode was field-free and the beam propagates with minimum magnetic deflection. (c) The propagation of ion beams through vacuum with cold electron neutralization was studied in a region well shielded from diode effects. (d) High ion-current densities, in excellent agreement with geometric predictions, were obtained at the focus.

Maximization of the ion-beam power density is of particular interest in relation to proposals for ion-beam-induced pellet fusion.³⁻⁵ Although, for ease of construction, the diode described was designed to produce a line focus, magnetically insulated diodes have potential for producing spherically converging beams, either with a single acceleration gap¹ or in a stacked configuration.

The experimental system is shown in Fig. 1. The goal was to design a high-current diode at

medium voltage to take advantage of the low-impedance output from the Neptune C generator.⁶ The geometry is cylindrical, with ions extracted inwards. The cylindrical cathode with slot extractors has an L/R time long compared to the magnetic-field risetime and thus excludes the field from the inner propagation volume, allowing the ions to approach closer to the axis. The

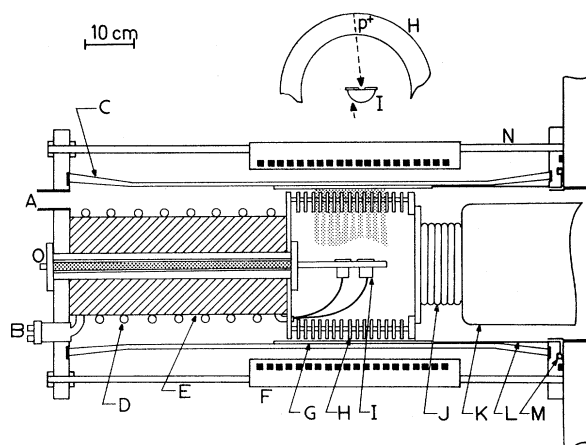


FIG. 1. Experimental apparatus: A, pumping port; B, diagnostic isolator output; C, glass vacuum vessel, 30 cm i.d.; D, diagnostic isolation inductor; E, Delrin support rod; F, 20-turn, 20-kG magnetic coil; G, anode; H, cathode assembly; I, ion-current-density probes; J, bellows for electrical connection; K, high-voltage terminal from the Neptune C generator; L, return conductors; M, Rogowski loop-current monitor; N, support rods; O, resistive diode-voltage monitor.

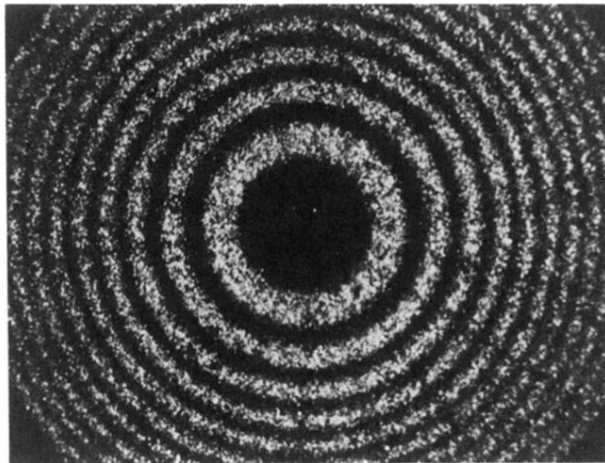


FIG. 1. Coded image of the α emission recorded on shot *B*. It is an array of more than one million pinholes (each produced by an α track) through the cellulose nitrate layer.